BULLETIN OF THE POLISH ACADEMY OF SCIENCES
TECHNICAL SCIENCES, Vol. 72(5), 2024, Article number: e150807
DOI: 10.24425/bpasts.2024.150807

Selected aspects of the operation of dual active bridge DC/DC converters

Serafin BACHMAN[1]*, **Marek TURZYŃSKI**[2], and **Marek JASIŃSKI**[1]

[1] Warsaw University of Technology, Institute of Control and Industrial Electronics, Poland
[2] Gdańsk University of Technology, Department of Power Electronics and Electrical Machines, Poland

Abstract. This review paper discusses the concept of a bidirectional dual active bridge (DAB) DC/DC converter. Practical applications and control methods are explored, and various types of DAB converters are introduced and characterized. Aspects of operation are discussed, and enriched by the results of theoretical analyses, simulations, and experimental measurements of the original authors' work.

Keywords: DC/DC converters; power electronic devices; dual active bridge converter; DC chargers.

1. INTRODUCTION

The increasing expansion of power systems using renewable energy sources has led to the emergence of novel concepts for power system development. One such example is the microgrid, where distributed energy sources such as wind farms and photovoltaic systems, energy storage, and loads are seamlessly integrated within a single microsystem. Commonly, microsystems can either be interconnected with the main power grid (on-grid) or operate independently in off-grid mode.

A distinct design of a microsystem is the DC-MG (DC microgrid), where power sources and receivers are linked to a shared bus powered by DC voltage (see Fig. 1). This design offers several key advantages including an easier integration of renewable energy sources with energy storage compared to systems using alternating voltage. Additionally, its improved power quality and stability eliminate the need for synchronizing renewable energy sources with the AC power grid and allow for more effective integration of receivers powered by DC voltage [1].

However, it should be noted that in the DC-MG microsystem, both energy sources and loads can operate at different voltage levels [2]. Moreover, for certain power sources (e.g., wind generators) and receivers, the essential operating voltage is alternating current. Consequently, receivers and power sources are connected to the main DC bus through appropriate power electronic converters. In the case of energy storage units, such as battery banks and supercapacitor banks, there is also a need to facilitate the two-way energy flow, i.e., from the bus to the storage unit in charging mode and from the storage unit to the bus in energy recovery mode. A similar requirement follows from employing electric vehicle batteries in vehicle-to-grid (V2G) mode, where the vehicle serves as a mobile energy store capable of releasing the stored energy to the DC-MG system. This solution contributes to enhancing system stability and power balance in the network and facilitates energy transfer in the opposite direction, corresponding to charging the battery of the electric vehicle [3].

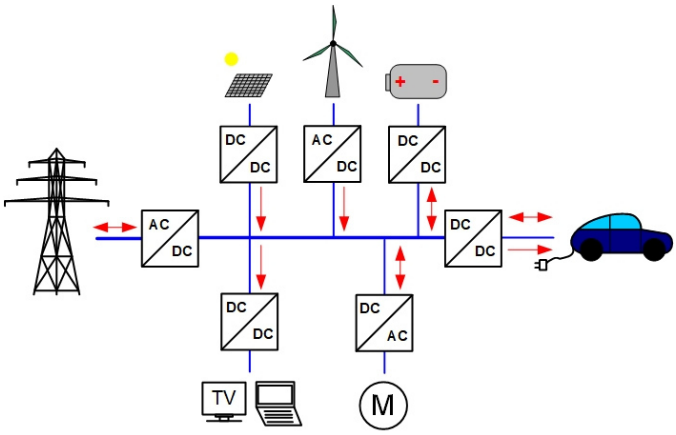

Fig. 1. DC microgrid (DC-MG) concept

As a result, the power electronic DC/DC converter that couples the DC bus and the storage unit should enable operation with varying levels of input and output voltages and support bidirectional transfer of energy. One of the systems meeting these requirements is the DC/DC converters in the dual active bridge (DAB) system.

The concept of the DAB converter was initially presented in 1988 [4]. The converter topology involves two full transistor bridges, H_1 and H_2 with feedback diodes (in single- or three-phase configurations), which are coupled using a high-frequency transformer with a winding ratio $n = N_2/N_1$ (see Fig. 2a) [5]. In currently adopted solutions, the switching frequency of transistors in converter bridges is not lower than several kHz. Consequently, the transformer cores of DAB systems are constructed using ferrite cores made of soft ferromagnetic materials like

*e-mail: serafin.bachman@pw.edu.pl

Manuscript submitted 2024-02-23, revised 2024-05-20, initially accepted for publication 2024-05-28, published in September 2024.

nickel-zinc or manganese-zinc sintered. It is noteworthy that issues related to the optimization of transformer parameters in DAB systems remain relevant, as they impact the ongoing development of this group of converters [6]. IGBT and MOSFET transistors are both used in the design of DAB converters, and ongoing research explores the use of semiconductor elements produced using SiC silicon carbide technology (commonly used in applications above 900 V) and GaN gallium nitride (in lower voltage applications) [7]. Additionally, L_d chokes can be employed to extend the current rise time and enhance the operating conditions of the system in the AC circuit.

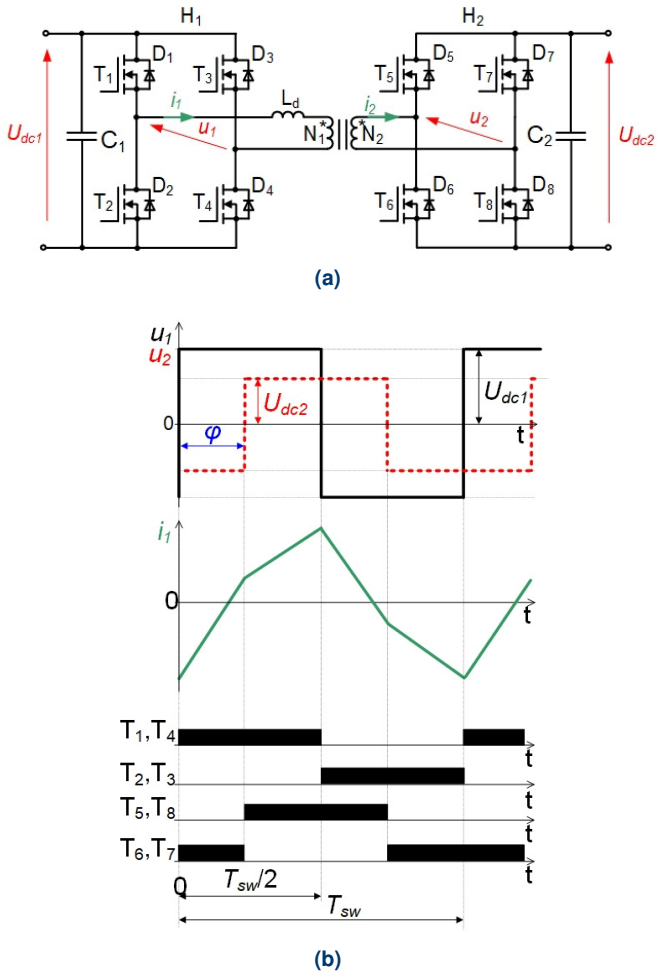

Fig. 2. Dual active bridge DC/DC converter (DAB): (a) scheme, (b) examples of waveforms

As a result of switching transistors in the converter bridges, voltage waves u_1 and u_2 are generated with an amplitude of U_{dc1} and U_{dc2}, respectively, which (ignoring losses) corresponds to the input and output voltage levels of the system (Fig. 2b). Influenced by the voltage acting on the magnetic components, currents i_1 and u_2 flow through the transformer windings, the waveforms of which depend on the phase shift angle φ between the voltage waveforms u_1 and u_2 and on the difference in the instantaneous values of the voltages u_1–u_2. The value of the output power of the Pout converter when transmitting energy from the H_1 to H_2 bridge is then expressed as [5]:

$$P_{\text{out}} = \frac{nU_{\text{dc1}}U_{\text{dc2}}\varphi(\pi-\varphi)}{2\pi^2 F_{sw} L_{\text{eq}}}, \tag{1}$$

where $F_{sw} = 1/T_{sw}$ – transistor switching frequency (several dozen – several hundred kilohertz for SiC systems), n – transformer turn ratio, L_{eq} – total inductance, which consists of the choke inductance L_d, the leakage inductance of the transformer primary winding (on the H_1 bridge side) and the leakage inductance of the secondary winding of the transformer related to its primary side.

According to equation (1), the output power Pout reaches its maximum value when the phase shift angle φ is $\pi/2$.

2. APPLICATION EXAMPLES OF DOUBLE ACTIVE BRIDGE CONVERTERS – DAB

The main advantages of DAB systems include a simple design, high efficiency of up to 98%, bidirectional energy transfer using the same control strategy regardless of the direction of energy transfer, high specific power density, the possibility of soft switching of the system transistors, a small number of passive elements, and galvanic isolation between the input and output of the converter [8–11]. As a result, DAB converters find applications not only in distributed generation and DC-MG systems but also in dedicated electric vehicle charging systems, autonomous power supply systems for electric vehicles, and as converters collaborating with energy storage devices [3, 12, 13].

An interesting application example, proposed in [14], is of DAB converters integrated into the structure of a traction substation in a low-voltage urban traction network (Fig. 3). One converter is responsible for powering the traction network, while the other serves as a charging or discharging system for the electric vehicle battery, corresponding to the V2G mode. Both

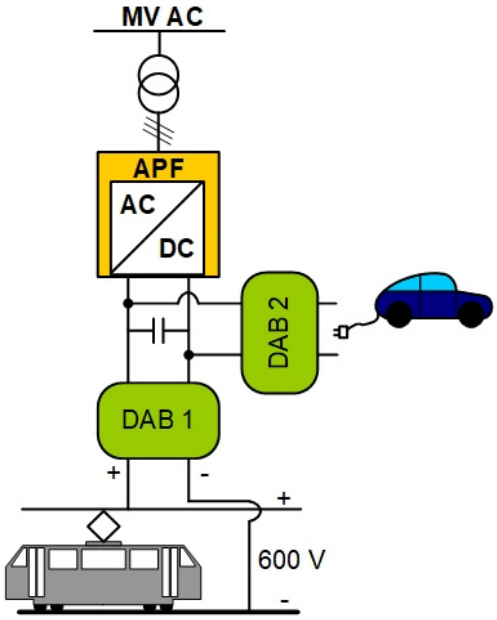

Fig. 3. The low voltage traction substation system proposed in [14]

DAB converters facilitate bidirectional energy flow between the overhead contact line and the vehicle battery. The entire system is powered by the medium voltage power grid via a network transformer, an APF (active power filter) filter, and an AC/DC converter. In cases where the voltage drops due to the start of vehicles powered by the traction network, the temporary energy deficiency can be compensated by drawing energy from the battery connected to the electric vehicle system. Similarly, additional energy generated during the braking of the traction vehicle and the recuperation process can be directed to the vehicle battery, contributing to the stabilization of the operating conditions of the traction network.

It is worth noting that power networks supplying electric traction systems face a noticeable problem of reactive power compensation at night when the energy consumption of traction vehicles is minimal. Consequently, there is a need for additional reactive power compensators. Charging stations for traction vehicles can serve a similar purpose, increasing active energy consumption, especially at night. While the solution proposed in [14] does not eliminate the need for reactive power compensators entirely, it does help reduce their size and overall cost.

One of the advantages of DAB systems is the ability to connect converters in series and parallel configurations, leading to the creation of modular converters (power electronics building block – PEBB), a concept proposed by American aircraft carriers in the 1960s. In this scenario, the output power of the modular converter depends on the power of a single elementary converter and the number of modules. In the context of DAB converters, the IPOS (input series output parallel) configuration, has proven particularly useful and finds application, among other areas, in traction systems.

For instance, in [15], a modular converter in the IPOS system consisting of 4 DAB converters was utilized to couple the battery with the main 2800 V DC bus, creating an auxiliary power source with a capacity of 183 kW for a Bombardier electric locomotive (Fig. 4a). The power of a single module, comprising a DAB converter, was defined to be 50 kW. The U_1 voltage measured at the battery terminals was anticipated to vary within the range of 518–835 V. Consequently, a parallel configuration of module connections was adopted on the U_1 voltage side, while a series configuration was employed on the Uh voltage side measured at the main terminals of the DC buses (2800 V–4200 V) (Fig. 4b) [15]. In another solution, it was proposed to connect eight DAB converters in the IPOS configuration to power DC traction systems [15]. The total power of such a modular converter was specified to be 1.25 MW with an input voltage of 25 kV (3125 V for a single module) and an output voltage of 1500 V. This system is currently under ongoing research.

The adoption of a modular system facilitates a simple configuration of the converter parameters based on current requirements by selecting the number of component modules. Moreover, in comparison with traditional systems, the maximum values of currents and voltages affecting the system elements in each module, and the required values of the maximum transmitted power are reduced, which helps mitigate the requirements placed on magnetic components and semiconductor elements, resulting in cost reduction and increased reliability of the converter.

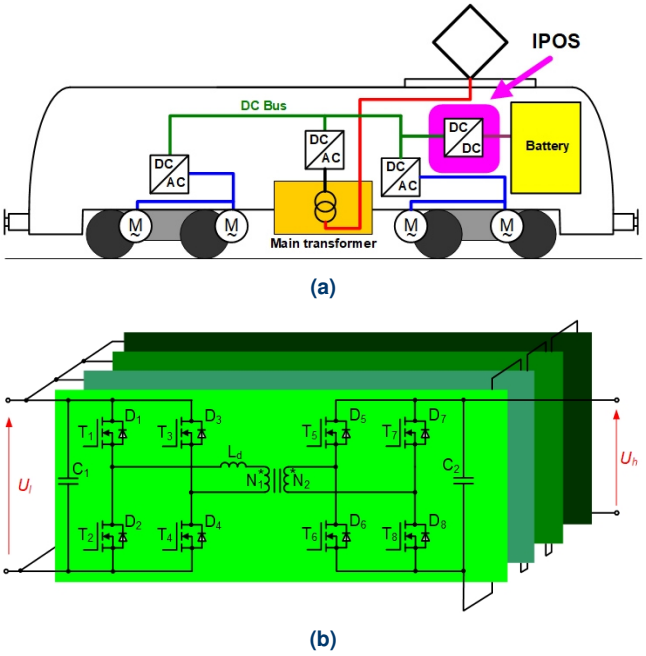

Fig. 4. (a) The concept of an electric locomotive with an additional energy storage tank, (b) a modular DC/DC converter in IPOS configuration [15]

Another area of application for DAB converters is in power electronic transformers (PETs). Similarly to classic power transformers, PET systems facilitate energy transfer between two alternating voltage circuits with the ability to shape the voltage value on the secondary side of the transformer while maintaining galvanic separation. The schematic diagram of the PET system (Fig. 5a) includes two AC/DC converters, with one used as a rectifier and the other - as an inverter, and a DAB system enabling energy transfer from the rectifier to the inverter [16]. Bidirectional converters in PET systems allow for energy transfer in both directions.

Compared to classic power transformers, PET systems feature smaller dimensions and the ability to control the flow of active and reactive energy with a low level of harmonic distortion. Moreover, they help limit the impact of load fluctuations on the power grid [17] and have a lower environmental impact due to the absence of oil, which is typically present in classic power transformers [17]. The efficiency of PET converters reaches 95%. In medium and high-power systems for medium and high-voltage network applications, cascade connection configurations are proposed to lower the exposure and requirements placed on the elements in a single module [18, 19] (Fig. 5b, 5c). A special area of PET applications is in traction, where power electronic transformers serve as an alternative to classic traction transformers. Ultimately, PET systems for traction applications aim for a power density of 1 kVA/kg, allowing for the installation of the converter in the chassis or on the roof of traction vehicles [20].

Other potential areas of PET application include the electricity distribution sector, renewable energy sources, industrial applications, and high-power drive applications [16, 18]. It should

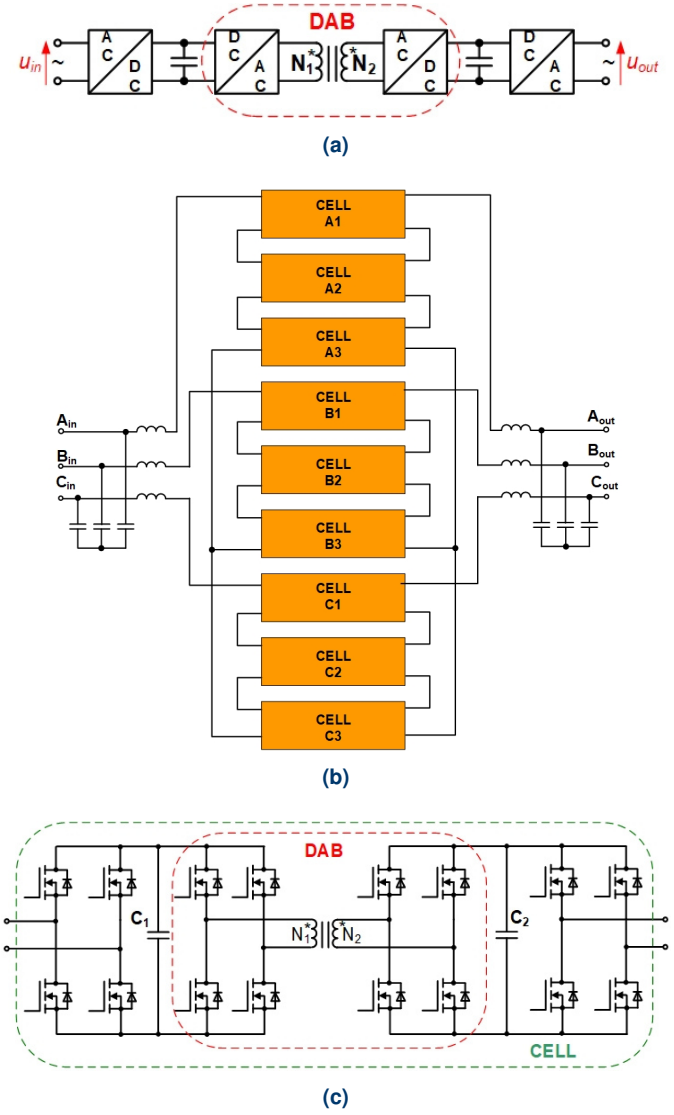

Fig. 5. Power electronic transformer (PET): (a) block scheme, (b) cascade topology of PET proposed in [18], (c) scheme of a single cell in PET [18]

be noted, however, that compared to classic power transformers, PET converters are characterized by a high degree of complexity with a large number of components (power electronic components, passive components, electronic components for control and monitoring, cooling system, etc.), which significantly affect reliability, availability, and maintenance costs [20].

3. EXAMPLE CONFIGURATIONS OF DAB SYSTEMS

Basic configurations of DAB systems include single-phase and three-phase topologies, with three-phase systems specifically designed for higher power applications. Nonetheless, ongoing research is exploring single-phase high-power converters, illustrated by the solution with a maximum power output of $P_{\text{out}} = 1$ MW and voltage levels of 12 kV/1.2 kV, presented in [21]. A comparison of single-phase and three-phase system topologies is provided later in this study. Proposed transistor bridge configurations encompass both classic full single- or three-phase bridges with four or six transistors, and multilevel solutions, particularly tailored for applications in PET systems [22].

A notable development in DAB converters is the shift towards resonant systems, where additional L_c resonant circuits facilitate soft switching of power electronic switches in zero current switching (ZCS) or zero voltage conditions (zero voltage switching, ZVS). Consequently, compared to hard commutation systems, commutation losses are reduced, contributing to improved energy efficiency. Furthermore, the reduction in the steepness of the commutation waveforms of currents and voltages leads to a decrease in the level of emitted electromagnetic disturbances.

The modification of the DAB system to a resonant converter configuration is commonly achieved by adapting known previous solutions, as illustrated in [21,23], in the DAB-SRC system, where a series resonant circuit in the configuration known from DC/DC converters of the SRC type (series resonant converters – SRC) is connected between the transistor bridge and the primary winding of the transformer (Fig. 6a). This configuration allows for soft switching of the transistors in the H_1 bridge in ZVS conditions and ZCS conditions for the switches in the H_2 bridge during energy flow from H_1 to H_2 bridge [21]. Moreover, compared to the hard commutation configuration, the shape of the transformer current is improved due to the reduction of higher harmonic content, further facilitating loss reduction [23].

Other proposed solutions for resonant DAB systems use a resonant circuit configuration taken from LLC converters [24,25]. Similar to SRC systems, the resonant circuit of DAB-LLC converters is connected between the bridge and the transformer winding (Fig. 6b). With the energy flow from H_1 to H_2 bridge and the transistor switching frequency higher than the resonant frequency F_r, the resonant circuit is inductive, resulting in ZVS conditions for the switches in the H_1 bridge and ZCS conditions for the switches in the H_2 bridge. It should be noted that the typical control method, by changing the phase shift angle φ, is ineffective in the case of the DAB-LLC system. Therefore, methods based on changing the fill factor value at a constant frequency F_{sw} or by changing the switching frequency of the transistors F_{sw} are recommended. Since the output voltage of the DAB-LLC system depends on the ratio of the resonant impedance of the resonant circuit to the load resistance, for a frequency F_{sw} higher than approximately $1.5F_r$, no further influence of F_{sw} on the output voltage is observed [25]. Consequently, control methods based on changing the duty cycle are recommended; however, at low duty cycle values, ensuring soft switching of the switches in the H_1 bridge may be challenging, prompting the proposal of asynchronous modulation [25]. Additionally, due to the asymmetry of the alternating current circuit of the DAB-LLC converter, when transmitting energy from the H_2 bridge to H_1, the transistors in the H_2 bridge are disabled under hard conditions, increasing commutation losses and reducing system efficiency. To address this, symmetrical topologies are proposed, employing resonant circuits on both sides of the transformer, as implemented in DAB-CLLC systems [26] (see Fig. 6c). While

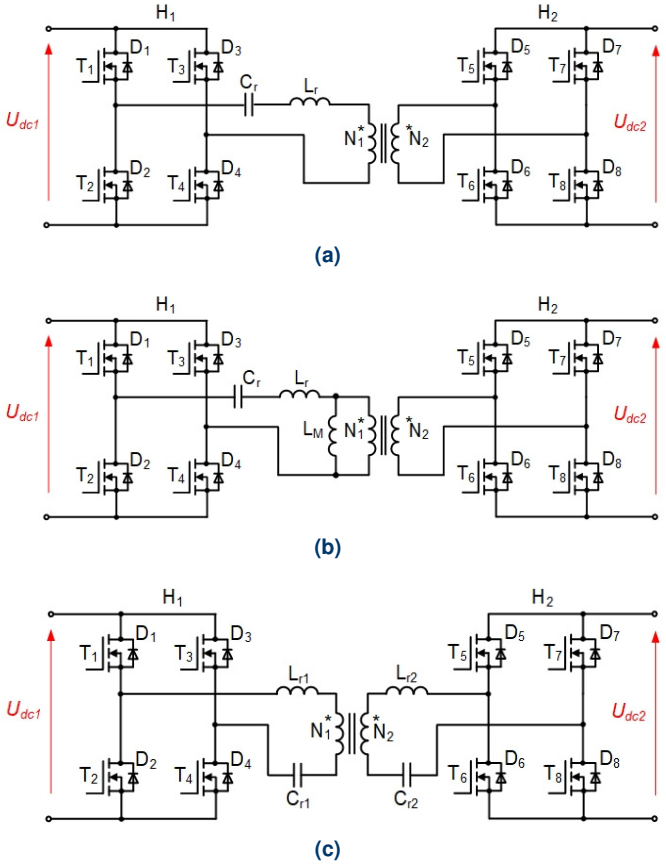

Fig. 6. Different resonant DAB converters: (a) DAB-SRC [23], (b) DAB-LLC [24], (c) DAB-CLLC configuration with symmetrical resonant tank [26]

these solutions ensure soft switching regardless of the direction of energy flow, the higher complexity of the topology, along with challenges in control and parameter selection, limits their practical application.

4. SELECTED ASPECTS OF THE OPERATION OF DAB CONVERTERS

The upcoming sections explore various aspects of the DAB converter operation, in a condensed format, including a comparison of the properties of single-phase and three-phase systems, considerations of issues related to soft switching of the converter transistors, an overview of basic control methods, and an examination of starting currents and the impact of selected DAB converter parameters on system characteristics. Additionally, an original control concept featuring a closed control loop with a current-voltage PI controller and modified DPS (double phase shift) modulator will be introduced. The discussion is complemented by original experimental results gained from the author's classic DAB converters in single- and three-phase configurations, constructed using semiconductor components made with SiC silicon carbide technology. The parameters of the experimental systems are outlined in Table 1. The voltage levels presented in Table 2 refer to the operation of the system in two

Table 1
Basic parameters of DAB 1-phase and 3-phase converters

Feature	DAB 1-phase	DAB 3-phase
Power (total)	10 kW	10 kW
Input voltage	600 V/380 V	600 V/380 V
Output voltage	380 V	380 V
Switching frequency	50 kHz	50 kHz
Transistors and diodes	F423MR12W1M1B11 (Infineon) CoolSiC™Trench MOSFET	F423MR12W1M1PB11 (Infineon) CoolSiC™Trench MOSFET
Inductance L_d	25 µH	25 µH
Transformer	3C95 ferrite core (SMA) $O_D = 87$ $I_D = 56$ $H = 50$ mm	3× 3C95 ferrite core (SMA) $O_D = 87$ $I_D = 56$ $H = 50$ mm

variants, with a transformer ratio of 1 and a ratio of 1:1.57, in two directions of operation.

The control system of the tested converters employs a DSP platform coupled with FPGA programmable logic systems, developed at the Institute of Control and Industrial Electronics of the Warsaw University of Technology. Power for the systems was supplied by the ITECH IT6018B power supply, with the High-Power DC Electronic Load ITECH IT8954A converter serving as the load for the tested DAB converters (Fig. 7).

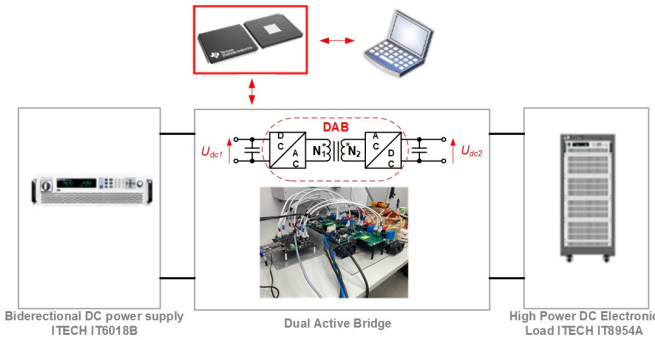

Fig. 7. Test bench configuration

4.1. Modulation aspect in dual active bridge control

An influential factor shaping the properties of DAB converters is the choice of the appropriate control strategy. One of the widely employed methods for controlling DAB converters is based on adjusting the phase shift angle (φ) between the voltage waveforms u_1 and u_2. This is achieved by time-shifting the switching moments of corresponding pairs of transistors in bridges H_1 and H_2 (Fig. 8b) – SPS [6, 27]. The dynamic properties of systems controlled using the SPS strategy are favorable, and the method itself is characterized by a low degree of complexity, making it practical for implementation, also in multiphase systems [28]. However, its application results in the generation of

high circulating currents between bridges resulting in high reactive power, even with a small converter load. This leads to an increase in the flow of reactive power, elevated current exposure of system components, and higher peak values of the current flowing through semiconductor and magnetic components, ultimately causing increased losses and reduced energy efficiency of the system [29]. Additionally, the permissible range of changes in the phase shift angle φ, where soft switching of the system transistors is possible, is relatively narrow, resulting in hard switching of the system transistors and a further loss escalation.

To mitigate the drawbacks of the SPS method, alternative control strategies have been proposed. One such strategy is the extended phase shift (EPS), which is a modification of SPS introducing two angles: φ (external) and φ_1 (internal). The latter introduces a phase shift between signals controlling the diagonal transistors in the primary bridge H_1 (Fig. 8c). The EPS method significantly reduces circulating currents in the AC circuit, leading to decreased reactive power and peak current values in the AC circuit compared to the SPS method. However, the disadvantage of the EPS method is its asymmetric control, necessitating a review of the transistor switching strategy for the opposite direction of energy transfer, resulting in, approximately, a 0.5–1% improvement in converter efficiency compared to SPS [30].

To further reduce reactive energy flow in the AC circuit and enhance energy efficiency, the double phase shift (DPS) control method is proposed. This method introduces an additional internal angle φ_2 for the signals controlling the transistors in the H_2 bridge (Fig. 8d). The DPS method is based on the equation: $\varphi_1 = \varphi_2$, thus providing two degrees of freedom in control. Publications claim up to a 2% increase in converter efficiency compared to the SPS method when using DPS [31].

An extension of the DPS method is the triple phase shift (TPS) strategy, allowing different values for shifts φ_1 and φ_2, resulting in a control method with three degrees of freedom (see Fig. 8e). Implementing the TPS strategy can lead to further improvements in converter energy efficiency – approximately 2.5% compared to the SPS method, based on our numerical results. However, it introduces complexity, and the same output power can be achieved with different combinations of φ, φ_1, and φ_2. Therefore, optimization criteria should be adopted, such as minimizing losses in magnetic components or limiting switching losses [32]. The TPS method is characterized by high complexity, potentially hindering practical implementation and wider applications.

It is worth noting that DAB control methods are currently evolving rapidly. One proposed direction is the development of hybrid methods, combining basic methods (SPS, DPS, and TPS) with the choice of the control strategy depending on the current operating conditions of the system [33]. At the current stage, the authors have selected the SPS and DPS methods for a single-phase system and SPS for three-phase systems as control strategies for experimental DAB systems.

In designing DAB converters, ensuring soft switching of transistors without the need for additional resonant circuits is crucial. In the DAB converter system, currents i_1 and i_2 flowing through the transformer windings are inductive (Fig. 2). Achieving soft

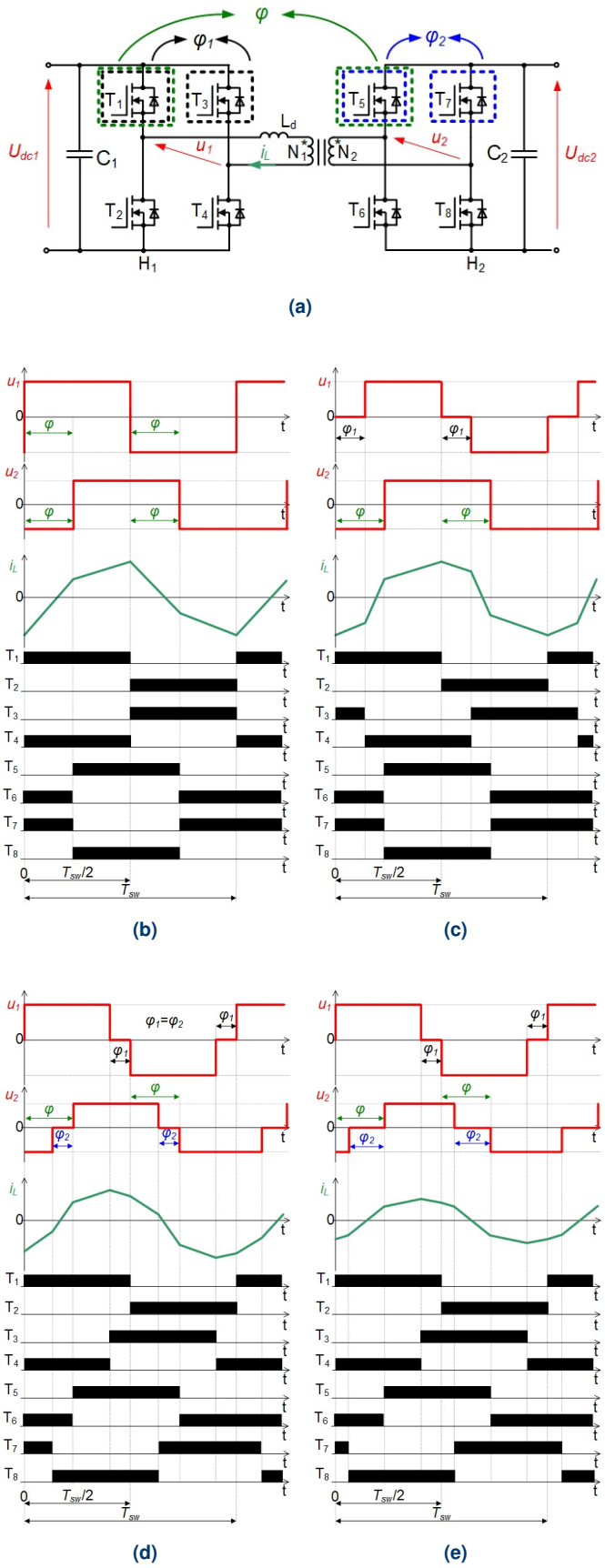

Fig. 8. Control strategies of DAB converter: (a) scheme, (b) SPS, (c) EPS, (d) DPS, (e) types

switching of the transistors involves overcharging capacitances connected in parallel with the switches. Parasitic capacitances of transistors or additional capacitors connected in parallel can serve this purpose (Fig. 9). The overcharging process allows for soft disengaging of the transistors, reducing the steepness of voltage waveforms and enabling ZCS/ZVS conditions. This method has been widely used in DAB systems, facilitating soft disengaging of transistors in both converter bridges irrespective of the direction of energy flow [34–36].

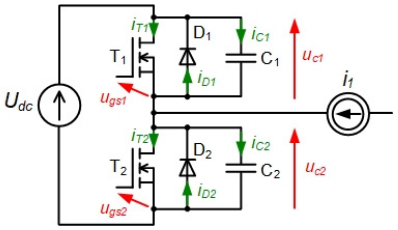

Fig. 9. Transistor soft turn-off in a converter bridge leg with additional parallel capacitances. Deeper waveform discussion in [36]

Soft switching in the DAB system is ensured by selecting the appropriate value of dead time, which must be correlated with the value of the designed series inductance so that the switched current is sufficient to overload the parallel capacitance and the transistor capacitance. Based on the research and analyses carried out for the classic method of controlling a DAB converter using the modulation method with a single phase shift modulation an example range of correct soft switching of the converter was determined and is presented in Fig. 10. The width of the characteristic area in which the soft switching occurs is based on the combination of parameters such as voltage ratio, current value, series inductance, and switching frequency. An important parameter determining the width of the ZVS switching area is the voltage ratio of the DAB converter k_u, defined as:

$$k_u = \frac{n U_{\mathrm{dc1}}}{U_{\mathrm{dc2}}}. \tag{2}$$

Determining the range of characteristics in which soft switching of the converter transistors is possible can be made based on the

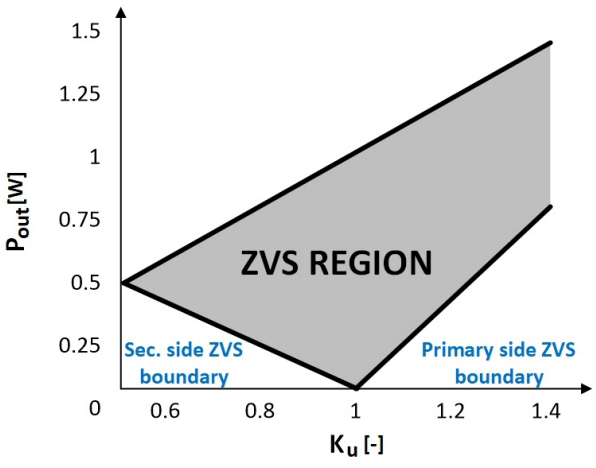

Fig. 10. Zero voltage switching (ZVS) region characteristic

relationships presented in [37], which ultimately determine the range of changes in the phase shift angle φ:

$$\varphi > \frac{\left(1-\frac{1}{k_u}\right)\pi}{2} \quad \text{and} \quad \varphi > \frac{(1-k_u)\,\pi}{2}. \tag{3}$$

Examples of oscillograms illustrating the soft switching of transistors in the experimental DAB system are shown in Fig. 11.

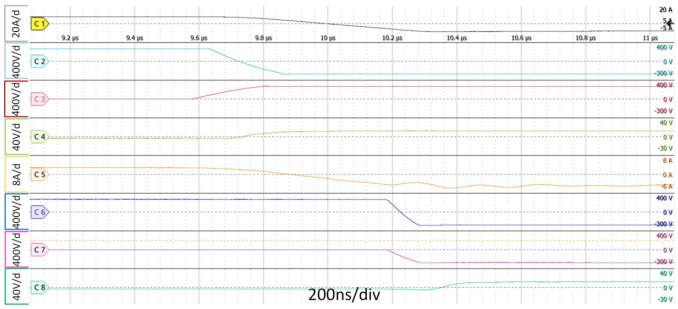

(a)

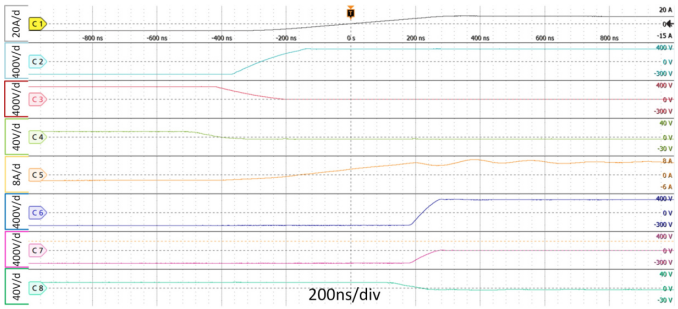

(b)

Fig. 11. Soft switching of DAB transistors (transistor designations as in Fig. 2), (a) rising edge of the upper transistor, (b) falling edge of the upper transistor. From the top: C1 – current of the primary side series inductor Ld (I_1), C2 – voltage of the primary side transformer (U_1), C3 – voltage of the transistor T1 drain-source (U_{c1}), C4 – gate voltage of the transistor T2 drain-source (U_{c2}), C5 – current of the secondary side transformer (I_2), C6 – voltage of the secondary side transformer (U_2), C7 – voltage of the transistor T5 drain-source, C8 – gate voltage of the transistor T6 drain-source, 200 ns/div and 4 us/div

DAB converters, whether single-phase or three-phase, share a similar structure and the ability to control output power through one or more phase shifts. Consequently, both systems can be governed by control loops of identical structures. The primary distinction in the control loops for these systems lies in the phase shift equation derived from the power equation.

Control methods are grounded in the application of a single or cascade proportional-integral (PI) controller. However, since the control characteristics of the DAB converter are non-linear, operating with linear characteristics is crucial for the stability of the control loop. To address this, linearization methods are employed [38]. One straightforward approach involves restricting the range of changes in the phase shift angle φ solely to

the linear range of the characteristic and adjusting the system parameters based on the modified power equations [38].

Another method for linearizing DAB characteristics is presented in [37]. This approach simplifies the DAB control characteristics by excluding intervals where the angle φ reaches significant values and eliminating points in the characteristic where distortions occur due to phenomena related to dead time (inactive conduction state, drift, voltage dips on elements, etc.). This linearization facilitates the direct calculation of the angle φ from the desired value of the converter output current $I_{\mathrm{dc2(ref)}}$ [39]:

$$\varphi = 0.25\left(1 - \sqrt{\frac{I_{\mathrm{dc2(ref)}}}{nI_n}}\right), \tag{4}$$

where I_n is the rated output current of the converter at the rated power P_n.

The simplest closed-loop control variant involves a single proportional-integral (PI) controller operating in a closed current loop. While this solution implementation is simple and features high dynamics, it requires additional protection in case of a load disconnection. In such scenarios, the regulator may enter a saturation state, leading to an increase in voltage on the secondary side of the converter due to the continuous supply of energy to the output capacitance. To address this, a combined voltage-current control loop can be employed, eliminating the drawbacks of a system with a single current regulator. However, this comes at the expense of reduced dynamics and increased complexity in the control system.

Building on original simulation and experimental research, a more advanced control method was developed to significantly enhance the flexibility of using the DAB system. By incorporating a control loop selection term, application flexibility is raised. This system can operate as a current, current-voltage, or current-power loop depending on the system state, adjusting to current operating conditions. The structure and configuration of this proposed control system are discussed in more detail in [38]. The proposed control system structure is illustrated in Fig. 12, while Fig. 13 displays exemplary current and voltage waveforms in an experimental DAB system controlled according to the author's proposal. Notably, despite the change in the set current value from close to zero to 10A (C4 waveform), the converter output voltage remained unchanged (C6 waveform).

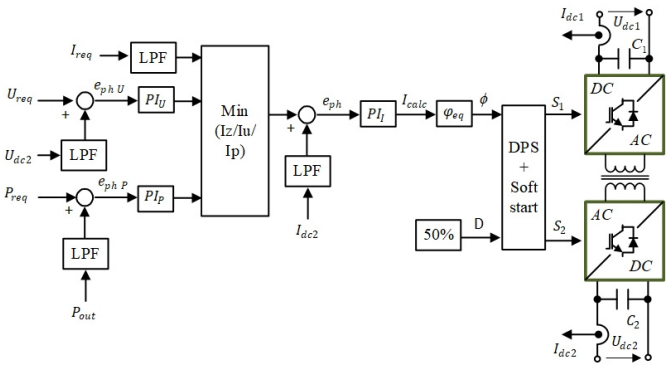

Fig. 12. Original control method using the soft-start method and the DPS modulator

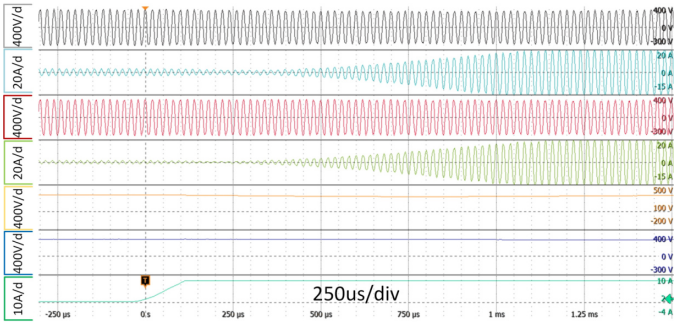

Fig. 13. Current and voltage waveforms in the DAB converter controlled in the system as in Fig. 12. From top: primary phase voltage (U_1), primary side phase current (I_1), secondary phase voltage (U_2), secondary side phase current (I_2), input DC voltage (U_{dc1}), output DC voltage (U_{dc2}), output load (I_{dc2}). The image shows a measurement aliasing problem which does not affect the edges of the DC part

An important concern related to converter operation is the reduction of starting currents. This issue arises from the occurrence of transformer overcurrent during system startup, leading to an overregulation of the phase current value on the secondary-side transformer to potentially dangerous levels. The root cause is the emergence of full-phase voltage at the AC terminals of the secondary side bridge with zero DC voltage on the secondary side. This phenomenon, observed during converter startup, results in a high starting current flowing through the magnetic components. Consequently, the current value may elevate to a level where the transformer core becomes saturated, introducing current distortion known in the literature as the "DC bias" [40]. The flow of a significant impulse current through the transistors in the secondary bridge may lead to damage. According to research on semiconductor reliability, subjecting semiconductor elements to cyclic current surges shortens their service life, contributing to lower converter reliability [41].

One proposed method for mitigating starting currents involves the use of the EPS modulation method. This method entails shaping the voltage waveform acting on the primary winding of the transformer, effectively limiting the rate of current increase [42] (Fig. 14).

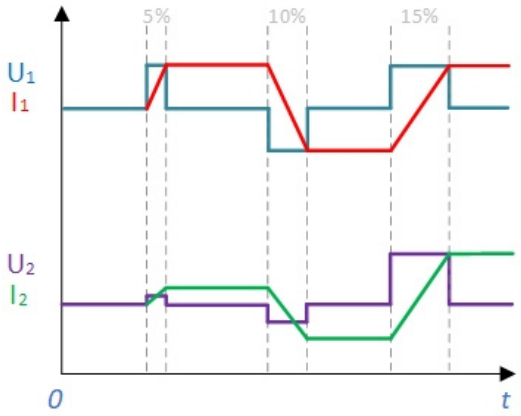

Fig. 14. DAB converter inrush current limitation method proposed in [42]

Limiting the current increase is accomplished by introducing a phase shift between the branches of the switches in the primary-side bridge (bridge H_1 when transferring energy from the bridge H_1 to H_2), akin to the EPS method (Fig. 8b). This results in a three-level characteristic of the voltage waveform on the primary side of the transformer (Fig. 15 – waveform C2). Modifying the voltage waveform serves to curtail the rate of increase of the phase current on the secondary side, eliminating current overshoots and ensuring the safe shaping of the secondary side current.

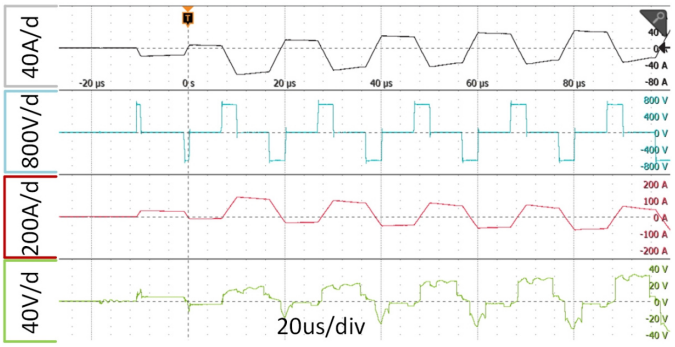

Fig. 15. Starting procedure of DAB. From top: current and voltage in the AC circuit at the primary side, current and voltage in the AC circuit at the secondary side

Figure 16 shows example waveforms illustrating the effectiveness of the starting current limiting method. In the case of starting without limiting the starting current (Fig. 16a), a notable high current overshoot with a characteristic offset reaching significant values is observed. On the other hand, an implementation of the proposed method (Fig. 16b) successfully limits the starting current, ensuring a safe startup of the converter.

4.2. Comparison of dual active bridge 1-phase vs 3-phase

The most prevalent DAB configuration is the single-phase topology (Fig. 17a), frequently employed in medium-power applications and at medium voltage levels [43,44]. Multi-phase topologies are primarily utilized in high-power applications, with the three-phase DAB converter being the most commonly employed configuration [45,46] (Figs. 17b, 17c). A comprehensive list of the fundamental characteristics of single- and three-phase systems is provided in Table 2.

Selecting the parameters of magnetic components is a critical step in achieving a stable DAB system. When designing a single-phase system, it is crucial to choose the appropriate leakage inductance, rated power, and circuit saturation current. For multiphase systems, these parameter values also depend on the adopted topology.

The total inductance value in a single-phase system can be determined based on the transformed relationship (1):

$$L_{\text{eq}} = \frac{\dfrac{U_{\text{dc1}} U_{\text{dc2}} \varphi(\pi - \varphi)}{2\pi^2 F_{sw}}}{P_n}, \tag{5}$$

where P_n is the rated power of the converter.

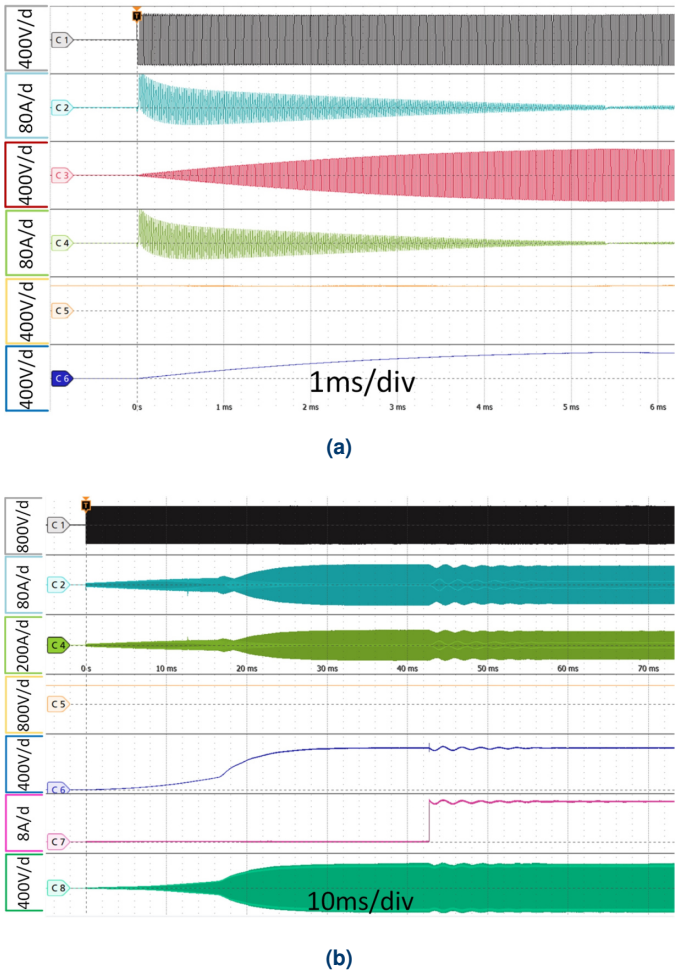

Fig. 16. DAB converter inrush operational waveforms: (a) without inrush current limitation, from top: C1 – primary phase voltage (U_1), C2 – primary phase current (I_1), C3 – secondary phase voltage (U_2), C4 – secondary phase current (I_2), C5 – DC input voltage (U_{dc1}), C6 – DC output voltage (U_{dc2}), (b) with inrush current limitation, from top: C1 – primary phase voltage (U_1), C2 – primary phase current (I_1), C8 – secondary phase voltage (U_2), C4 – secondary phase current (I_2), C5 – DC input voltage (U_{dc1}), C6 – DC output voltage (U_{dc2}), C7 – DC output current (I_{dc2})

However, in the case of three-phase systems, the inductance value for individual phases is:

$$L_{\text{eq}} = L_1 = L_2 = L_3 = \frac{7n U_{\text{dc1}} U_{\text{dc2}}}{8 F_{sw} P_n}. \tag{6}$$

Various transformer winding configurations are permissible in multiphase DAB converters. For instance, in three-phase systems, the most popular solutions are the star-star (Y-Y) (Fig. 17b) and star-delta (Y-D) configurations (Fig. 17c) [46]. While having the same main converter parameters, these topologies differ in the value of series inductance and the ratio of voltages and currents on the primary to secondary sides, which results from the adopted transformer configuration.

Additionally, the comparison of the current waveform for a single-phase system (Fig. 18a) and for a three-phase system

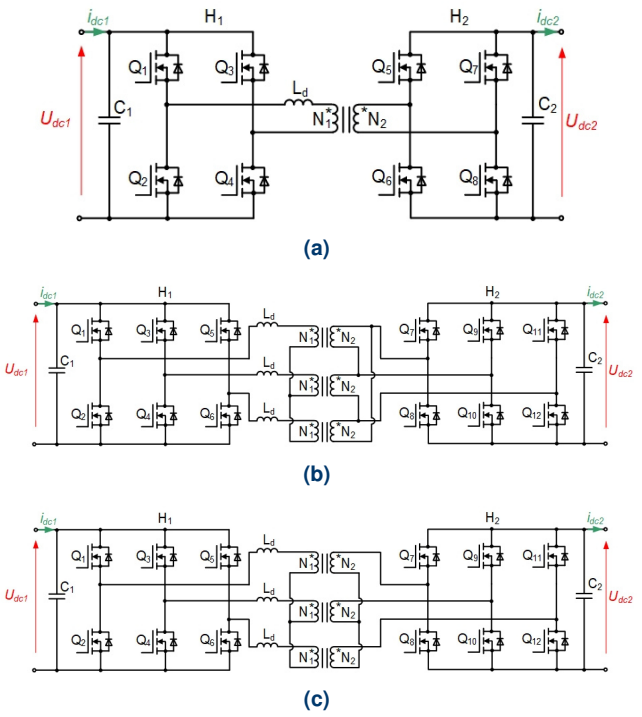

Fig. 17. Basic DAB topologies: (a) single-phase, (b) three-phase in star-star transformer topology (Y-Y), (c) three-phase in star-star delta topology (Y-D)

Table 2
Comparison of DAB 1-phase vs 3-phase

Feature	DAB 1-phase	DAB 3-phase
Cost	Low	High
Transistors	8	12
Magnetic circuit	A lower degree of complexity than in the 3f system	Complicated
Inrush current	High	Approx. 1/3 current value compared to the 1f equivalent
The shape of the current in an AC circuit	Trapezoidal	Less deformed
Level of emitted electro-magnetic disturbances EMI	High	Low
Efficiency	Max. 98%	Max. 97%
Capacitances in DC circuits	Low	High
Series inductance Leq	High	Low

(Fig. 18b), which adopts a much more sinusoidal shape, indicates the possibility of reducing emission levels through a simple change in topology.

Moreover, in the case of a star-star configuration (Fig. 20b), the shape of the current in the AC circuit is more trapezoidal,

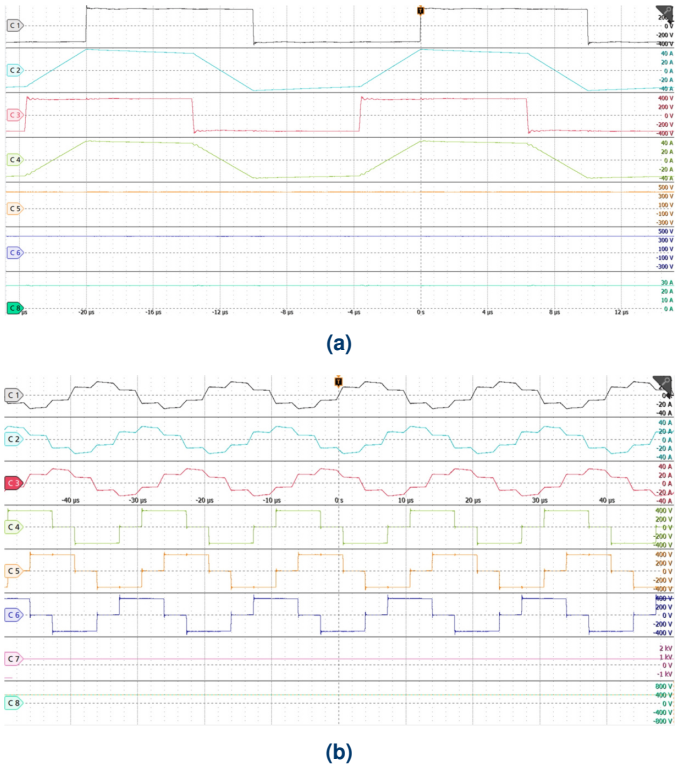

Fig. 18. Experimental waveforms of DAB DC/DC converter: (a) single-phase configuration. From top: C1–C2 primary phase voltage and current (U_1, I_1), C2–C3 secondary phase voltage and current (U_2, I_2), C7 – input DC link voltage (U_{dc1}), C8 – output DC link voltage (U_{dc2}); (b) three-phase star-star configuration. From top: C1–C3 phase currents (I_{1-3}), C4–C6 phase voltages (U_{1-3}), C7 – input DC link voltage (U_{dc1}), C8 – output DC link voltage (U_{dc2}), 10 us/div

whereas in the case of a star-delta system (Fig. 20a), the shape of the current is closer to sinusoidal [47]. This is further confirmed by the example distributions of higher harmonics for the current in the i_1 primary side of the transistor in H_1 bridge measured in experimental systems (Fig. 19).

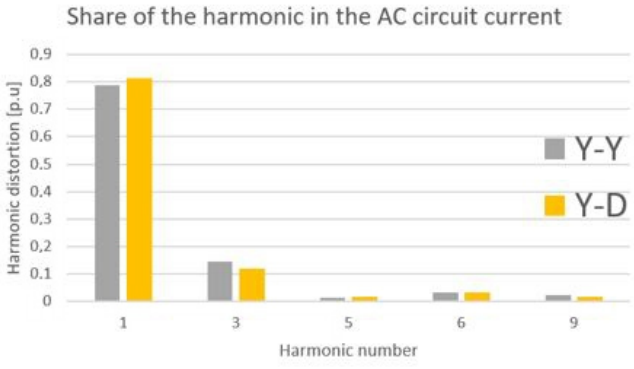

Fig. 19. Exemplary harmonic distribution of current in the AC circuit of DAB three-phase in the Y-Y configuration (orange) and three-phase in the Y-D configuration (gray)

It should be noted that in the case of a three-phase star-star configuration, the range of output voltage changes for a wide

range of output power is wider than in the Y-D system. However, this configuration is characterized by lower efficiency at lower loads, higher peak efficiency, and lower RMS values of the transformer current. The star-delta topology is characterized by a lower value of the required output capacitance, a larger content of higher current harmonics, a wider range of voltage changes for the low-load state, a wider operating range in which soft switching of the transistors is maintained, and lower values of generated electromagnetic disturbances EMI due to the less distorted shape of the transformer phase current. Example waveforms of the compared systems are presented in Fig. 18 and Fig. 20.

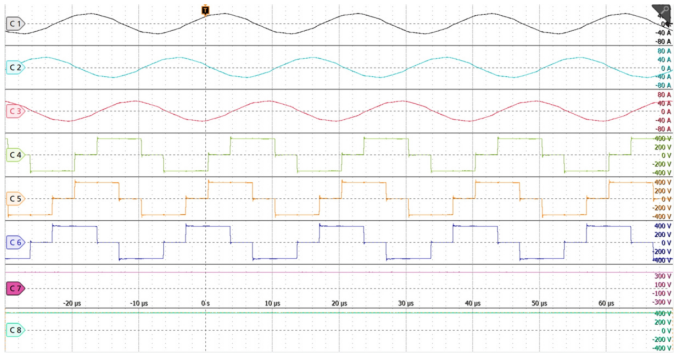

(a)

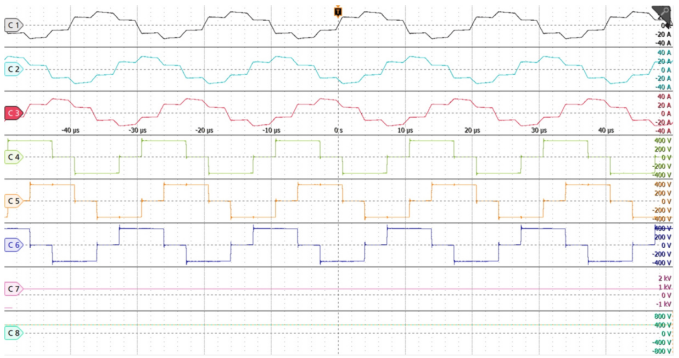

(b)

Fig. 20. Example operational waveforms of 10 kW three-phase DAB DC/DC converter. From top: C1–C3 phase currents (I_{1-3}), C4–C6 phase voltages (U_{1-3}), C7 – input DC link voltage (U_{dc1}), C8 – output DC link voltage (U_{dc2}): (a) star-delta(, (b) star-star, 10 us/div

An interesting aspect is the efficiency characteristics of DAB converters. The characteristics presented in Fig. 21 indicate the higher efficiency of the star-star topology. The system was tested for the same magnetic components in two configurations. For this reason, the change in topology resulted in a change in the voltage ratio, which may reduce the efficiency of the star-delta system. Moreover, the efficiency results of a single-phase and three-phase converter in the star-star and star-delta variants were compared. It should also be noted that in the case of system 1f, changing the control strategy from SPS to DPS results in an increase in system efficiency by approximately 1% at maximum output power.

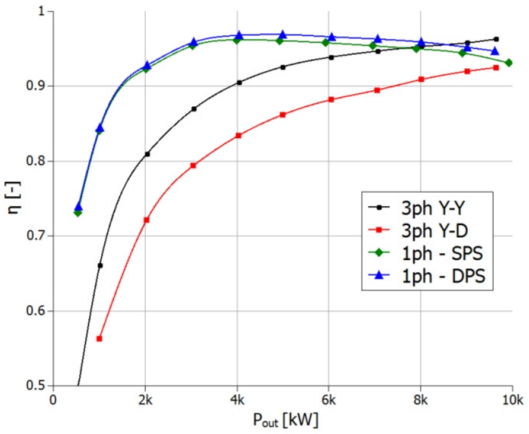

Fig. 21. Efficiency characteristics of DAB converters in single-phase, three-phase Y-D and three-phase Y-Y configurations

The lower efficiency values at low power stem from the ratio of losses in the magnetic circuit and semiconductor components. The design of the power circuit and the ratio of total losses to the relatively low output power results in such a characteristic being plotted in Fig. 21.

4.3. The influence of nonlinearity on the characteristics of DAB converters

Regardless of the adopted configuration, all types of DAB converters are characterized by a certain non-linearity of the control characteristics, compensated by various types of linearization of the characteristics [48–50]. Examples of the characteristics of the dependence of the output power on the phase shift angle φ for the SPS power control method are presented in Fig. 22. Figure 22a shows the influence of the leakage inductance Ll of the transformer winding, which accounts for an increase in Ll resulting in a significant decrease in the converter output power. Similarly, the value of the maximum output power of the converter also depends on the value of the adopted voltage ratio ku (defined in equation (2)). As the value of ku increases, the value of the output power for the same value of the angle φ also increases (Fig. 22b).

Similarly, the influence of dead time is also noticeable. In the event of a significant extension of the dead time value, subperiods may appear in the current waveform in the AC circuit in which i0. As a result, while maintaining the same value of the phase shift angle φ, supply voltage, and load resistance, the output power and output voltage decrease with the increase in the dead time value, which is particularly clear in the case of dead times longer than 0.02 Tsw (Fig. 23). The result presented in Fig. 23 is the optimum theoretical characteristic (the operation with dead time equal to 0 is possible in a simulation). As a result, it becomes necessary to compensate for the effect of dead time, for example, by increasing the phase shift angle φ. The failure to take dead time into account may result in a significant difference between the optimum and actual control characteristics of the DAB converter. In practice, minimal energy in the inductor Ll should be sufficient to replenish the energy stored in the parasitic capacitance of the transistor.

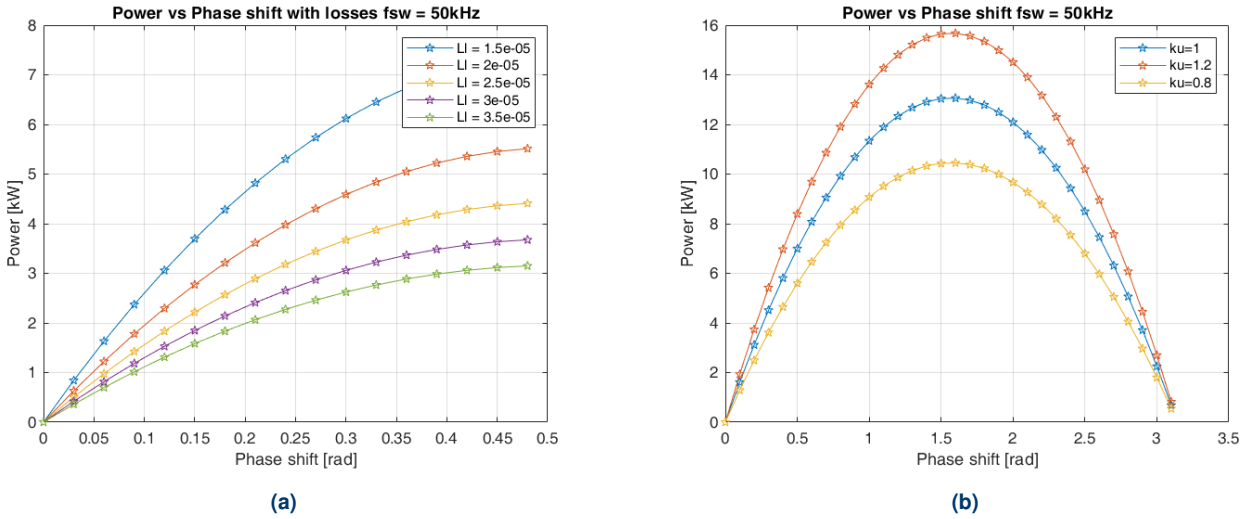

Fig. 22. Control characteristics of the DAB converter: (a) in dependence on the leakage inductance Ll, (b) in dependence on the voltage ratio ku. Losses were determined from Matlab calculations based on equation [37]

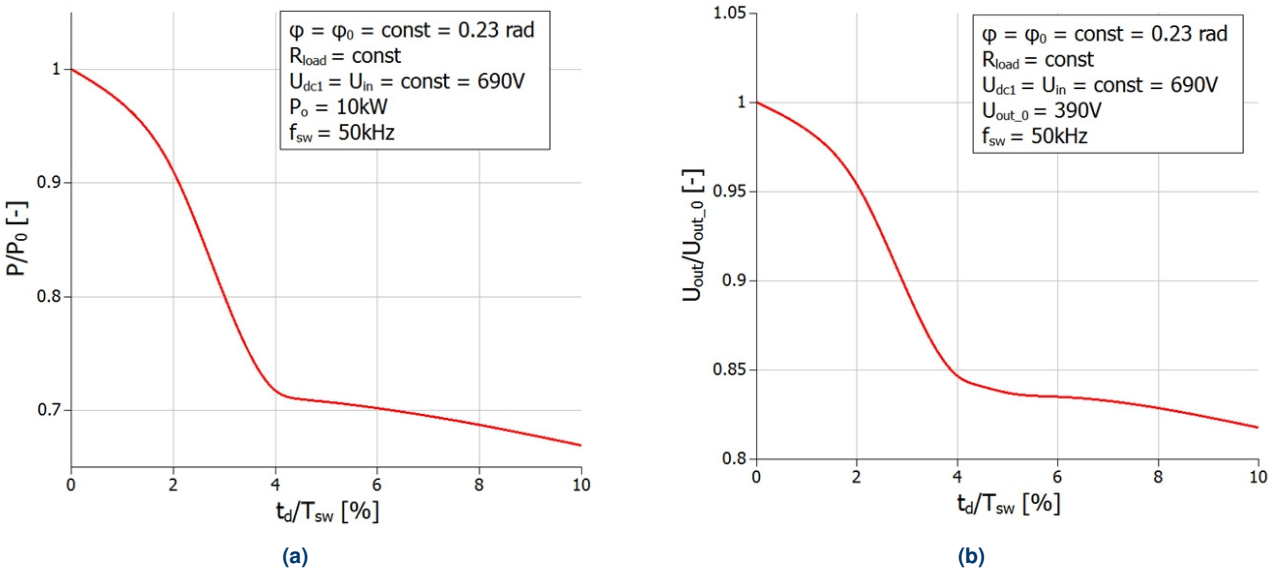

Fig. 23. Impact of the dead-time td: (a) on output power, (b) on output voltage

4.4. The influence of dead time on the characteristics of DAB converters

The evolution of DAB systems pivots on the advancement of multi-phase and multi-module topologies. Currently, a large number of configurations within this topology exist, each distinguished by substantial variations. Ongoing global research faces such challenges as mitigating circulating currents, expanding the characteristic range for soft switching, refining magnetic components, managing current surges and semiconductor diode losses, and enhancing synchronization and information exchange between converters.

Moreover, the maturation of research methodologies using artificial intelligence and neural networks holds the potential to usher in sophisticated, adaptive control methodologies tailored to relevant operational conditions. A pivotal area for technological development is in multi-module DAB systems, where disparities in energy flow direction or a lack of synchronization between pins may arise. DAB systems confer a notable advantage – the galvanic isolation of the input circuit from the output circuit, thereby bolstering user safety.

An indisputable challenge in the mass production of DAB systems lies in fabricating high-frequency induction elements, an area that has not yet been fully mastered. However, efforts are increasingly focused on automating and optimizing this process across a spectrum of voltages and powers [51]. Simultaneously, research is exploring various modifications to the converter topology [52]. Collectively, these initiatives foretell a highly promising future for this straightforward yet versatile topology.

5. CONCLUSIONS

The article extensively explores the utilization of dual active bridge (DAB) DC/DC converters, focusing on their application in microgrid systems and their increasing integration into contemporary power systems. The discussion includes detailed examples of applications, control methods, and characterizations of various types of DAB converters. Operational aspects such as modulator selection, proper converter startup methodology, comparison of single-phase and three-phase topologies, conditions for zero voltage switching, nonlinearities in converter characteristics, and the impact of dead time are also addressed.

In summary, when comparing the presented topologies, it can be noted that in terms of simplicity of implementation and the number of components, the 1-phase system excels. The 3-phase topology is characterized by higher power density. It is worth noting the current waveform in the star-delta configuration, is close to sinusoidal, hence it is expected higher harmonics and electromagnetic interference emissions reduction. The cost of and volume of 1-phase in comparison to 3-phase DAB is lower.

Future research is bound to explore and advance the control methodologies of DAB converters across diverse applications. The inherent modularity of DAB topology aligns seamlessly with the principles of power electronics building blocks (PEBB), facilitating serial and parallel connections of systems.

The article highlights the intriguing potential of DAB functioning as part of an intelligent power electronic transformer, offering high short-circuit resistance (via a traditional transformer in parallel) and swift responses to dynamic states such as load changes or asymmetry.

DAB converters emerge as a versatile technology with diverse applications spanning energy transformation, electromobility, renewable energy utilization, storage, and sustainable management. Given the vast scope of DAB applications, the authors plan to further investigate the possibility of developing an intelligent, personalized power electronic converter adept at seamless processing of both information technology (IT) and energy technology (ET).

Drawing parallels with the evolution of personal computers (PCs) from the second half of the 20th century to the present, the article speculates that the added capability of transforming AC/DC/DC electricity, manipulating currents and voltage levels, and enabling storage could provide a level of freedom unmatched by most current electrical and electronic devices. The dynamic progress in IT and ET technologies instills optimism for the rapid modernization of power systems, with personal and intelligent power electronic converters playing a pivotal role.

Funding

This research was financed from the 'Poland-Taiwan cooperation POLTAJ VII 7th competition Path 1' project, co-financed by the National Center for Research and Development.

REFERENCES

[1] M. Fotopoulou, D. Rakopoulos, D. Trigkas, F. Stergiopoulos, O. Blanas, and S. Voutetakis, "State of the Art of Low and Medium Voltage Direct Current (DC) Microgrids," *Energies*, vol. 14, no. 18, p. 5595, Sep. 2021, doi: 10.3390/en14185595.

[2] A.H. Sabry, A.H. Shallal, H.S. Hameed, and P.J. Ker, "Compatibility of household appliances with DC microgrid for PV systems," *Heliyon*, vol. 6, no. 12, p. e05699, Dec. 2020, doi: 10.1016/j.heliyon.2020.e05699.

[3] I. Skouros, A. Bampoulas, and A. Karlis, "A bidirectional dual active bridge converter for V2G applications based on DC microgrid," in *2018 Thirteenth International Conference on Ecological Vehicles and Renewable Energies (EVER)*, Monte-Carlo, Apr. 2018, pp. 1–9. doi: 10.1109/EVER.2018.8362396.

[4] R.W.A.A. De Doncker, D.M. Divan, and M.H. Kheraluwala, "A three-phase soft-switched high-power-density DC/DC converter for high-power applications," *IEEE Trans. Ind. Appl.*, vol. 27, no. 1, pp. 63–73, Feb. 1991, doi: 10.1109/28.67533.

[5] M. Turzyński *et al.*, "Analytical Estimation of Power Losses in a Dual Active Bridge Converter Controlled with a Single-Phase Shift Switching Scheme," *Energies*, vol. 15, no. 21, p. 8262, Nov. 2022, doi: 10.3390/en15218262.

[6] E.S. Lee, S.H. Song, J.H. Park, and M.R. Kim, "Optimal transformer design of DAB converters in solid-state transformers for maximum power efficiency," *IET Power Electron.*, vol. 16, no. 10, pp. 1625–1639, Aug. 2023, doi: 10.1049/pel2.12418.

[7] H. Beiranvand, E. Rokrok, and M. Liserre, "Volume Optimization in Si IGBT based Dual-Active-Bridge Converters," in *2019 10th International Power Electronics, Drive Systems and Technologies Conference (PEDSTC)*, Shiraz, Iran, Feb. 2019, pp. 577–582. doi: 10.1109/PEDSTC.2019.8697785.

[8] Y.V. Pushpalatha and D. Peftitsis, "Design of Dual Active Bridge Converters with SiC MOSFETs for minimized reflow power operation," in *2021 IEEE 12th Energy Conversion Congress & Exposition – Asia (ECCE-Asia)*, Singapore, May 2021, pp. 574–579. doi: 10.1109/ECCE-Asia49820.2021.9479059.

[9] N. Blasuttigh, H. Beiranvand, T. Pereira, S. Castellan, and M. Liserre, "Efficiency Trade-off-Oriented Analysis for the integration of DC-DC Converter and Battery Pack in V2G Applications," in *2022 IEEE Energy Conversion Congress and Exposition (ECCE)*, Detroit, USA, Oct. 2022, pp. 1–7, doi: 10.1109/ECCE50734.2022.9947733.

[10] M.F. Fiaz, S. Calligaro, M. Iurich, and R. Petrella, "Analytical Modeling and Control of Dual Active Bridge Converter Considering All Phase-Shifts," *Energies*, vol. 15, no. 8, p. 2720, Apr. 2022, doi: 10.3390/en15082720.

[11] B. Kwak, M. Kim, and J. Kim, "Inrush current reduction technology of DAB converter for low-voltage battery systems and DC bus connections in DC microgrids," *IET Power Electron.*, vol. 13, no. 8, pp. 1528–1536, Jun. 2020, doi: 10.1049/iet-pel.2019.0506.

[12] F. Krismer and J.W. Kolar, "Efficiency-Optimized High-Current Dual Active Bridge Converter for Automotive Applications," *IEEE Trans. Ind. Electron.*, vol. 59, no. 7, pp. 2745–2760, Jul. 2012, doi: 10.1109/TIE.2011.2112312.

[13] S.J. Ríos, D.J. Pagano, and K.E. Lucas, "Bidirectional Power Sharing for DC Microgrid Enabled by Dual Active Bridge DC-DC Converter," *Energies*, vol. 14, no. 2, p. 404, Jan. 2021, doi: 10.3390/en14020404.

[14] M. Lukianov, I. Verbytskyi, E.R. Cadaval, and R. Strzelecki, "Bidirectional EV charger integration into LV DC traction grid," in *2023 IEEE 17th International Conference on Compatibility, Power Electronics and Power Engineering (CPE-*

POWERENG), Tallinn, Estonia, Jun. 2023, pp. 1–8. doi: 10.1109/CPE-POWERENG58103.2023.10227489.

[15] M. Stojadinović and J. Biela, "Isolated DC-DC Converter for Battery Storage in Traction Applications: Modelling and Design of a Medium Frequency Transformer," *5th Swiss Competence Center for Energy Research Annual Conference (SCCER 2018)-poster*, Sep. 2018, doi: 10.3929/ETHZ-B-000365149.

[16] S. Falcones, R. Ayyanar, and X. Mao, "A DC–DC Multiport-Converter-Based Solid-State Transformer Integrating Distributed Generation and Storage," *IEEE Trans. Power Electron.*, vol. 28, no. 5, pp. 2192–2203, May 2013, doi: 10.1109/TPEL.2012.2215965.

[17] A. Rehman, M. Imran-Daud, S.K. Haider, A.U. Rehman, M. Shafiq, and E.T. Eldin, "Comprehensive Review of Solid-State Transformers in the Distribution System: From High Voltage Power Components to the Field Application," *Symmetry*, vol. 14, no. 10, p. 2027, Sep. 2022, doi: 10.3390/sym14102027.

[18] M. Morawiec and A. Lewicki, "Power electronic transformer based on cascaded H-bridge converter," *Bull. Pol. Acad. Sci. Tech. Sci.*, vol. 65, no. 5, pp. 675–683, Oct. 2017, doi: 10.1515/bpasts-2017-0072.

[19] M. Saeed, M.R. Rogina, A. Rodríguez, M. Arias, and F. Briz, "SiC-Based High Efficiency High Isolation Dual Active Bridge Converter for a Power Electronic Transformer," *Energies*, vol. 13, no. 5, p. 1198, Mar. 2020, doi: 10.3390/en13051198.

[20] S. Farnesi, M. Marchesoni, M. Passalacqua, and L. Vaccaro, "Solid-State Transformers in Locomotives Fed through AC Lines: A Review and Future Developments," *Energies*, vol. 12, no. 24, p. 4711, Dec. 2019, doi: 10.3390/en12244711.

[21] G. Ortiz, J. Biela, D. Bortis, and J.W. Kolar, "1 Megawatt, 20 kHz, isolated, bidirectional 12kV to 1.2kV DC-DC converter for renewable energy applications," in *2010 International Power Electronics Conference – ECCE ASIA*, Sapporo, Japan, Jun. 2010, pp. 3212–3219. doi: 10.1109/IPEC.2010.5542018.

[22] T. Gajowik, "Review of multilevel converters for application in solid state transformers," *Przegląd Elektrotechniczny*, vol. 2017, no. 4, pp. 3–7, Apr. 2017, doi: 10.15199/48.2017.04.01.

[23] P. Trochimiuk, R. Miśkiewicz, J. Rąbkowski, K.N. Kumar, and D. Peftitsis, "Experimental evaluation of SiC-based medium voltage Series Resonant Dual-Active-Bridge three-level DC/DC converters for EV charging," in *2023 IEEE 17th International Conference on Compatibility, Power Electronics and Power Engineering (CPE-POWERENG)*, Tallinn, Estonia, Jun. 2023, pp. 1–6. doi: 10.1109/CPE-POWERENG58103.2023.10227494.

[24] Y. Liao, J. Liang, D. Yang, K. Chen, J. Li, and Y. Yan, "Optimal Design Method of LLC-DAB Hybrid Bidirectional DC-DC Converter Based on Multi-objective Particle Swarm Optimization," in *2022 4th International Conference on Smart Power & Internet Energy Systems (SPIES)*, Beijing, China, Dec. 2022, pp. 250–255, doi: 10.1109/SPIES55999.2022.10082688.

[25] A. Hillers, D. Christen, and J. Biela, "Design of a Highly efficient bidirectional isolated LLC resonant converter," in *2012 15th International Power Electronics and Motion Control Conference (EPE/PEMC)*, Novi Sad, Serbia, Sep. 2012, p. DS2b.13-1-DS2b.13-8. doi: 10.1109/EPEPEMC.2012.6397282.

[26] J.-H. Jung, H.-S. Kim, J.-H. Kim, M.-H. Ryu, and J.-W. Baek, "High efficiency bidirectional LLC resonant converter for 380V DC power distribution system using digital control scheme," in *2012 Twenty-Seventh Annual IEEE Applied Power Electronics Conference and Exposition (APEC)*, Orlando, FL, USA, Feb. 2012, pp. 532–538. doi: 10.1109/APEC.2012.6165871.

[27] A. Rashwan, A.I.M. Ali, and T. Senjyu, "Current stress minimization for isolated dual active bridge DC–DC converter," *Sci. Rep.*, vol. 12, no. 1, p. 16980, Oct. 2022, doi: 10.1038/s41598-022-21359-1.

[28] J. Zeng, Y. He, Z. Lan, Z. Yi, and J. Liu, "Optimal control of DAB converter backflow power based on phase-shifting strategy," *Soft Comput.*, vol. 24, no. 8, pp. 6031–6038, Apr. 2020, doi: 10.1007/s00500-020-04715-z.

[29] B. Zhao, Q. Yu, and W. Sun, "Extended-Phase-Shift Control of Isolated Bidirectional DC–DC Converter for Power Distribution in Microgrid," *IEEE Trans. Power Electron.*, vol. 27, no. 11, pp. 4667–4680, Nov. 2012, doi: 10.1109/TPEL.2011.2180928.

[30] S. Fan, Y. Li, Y. Yuan, X. Hu, and W. Dai, "Comparative Analysis of Isolated Bidirectional Dual-Active-Bridge DC-DC Converter Based on EPS and DPS," in *2019 22nd International Conference on Electrical Machines and Systems (ICEMS)*, Harbin, China, Aug. 2019, pp. 1–6, doi: 10.1109/ICEMS.2019.8921569.

[31] B. Zhao, Q. Song, and W. Liu, "Power Characterization of Isolated Bidirectional Dual-Active-Bridge DC–DC Converter with Dual-Phase-Shift Control," *IEEE Trans. Power Electron.*, vol. 27, no. 9, pp. 4172–4176, Sep. 2012, doi: 10.1109/TPEL.2012.2189586.

[32] M. Capó-Lliteras, G.G. Oggier, E. Bullich-Massagué, D. Heredero-Peris, and D. Montesinos-Miracle, "Analytical and Normalized Equations to Implement the Optimized Triple Phase-Shift Modulation Strategy for DAB Converters," *IEEE J. Emerg. Sel. Top. Power Electron.*, vol. 11, no. 3, pp. 3535–3546, Jun. 2023, doi: 10.1109/JESTPE.2023.3236097.

[33] J. Sun, L. Qiu, X. Liu, J. Zhang, J. Ma, and Y. Fang, "Improved Model Predictive Control for Three-Phase Dual-Active-Bridge Converters with a Hybrid Modulation," *IEEE Trans. Power Electron.*, vol. 37, no. 4, pp. 4050–4064, Apr. 2022, doi: I10.1109/TPEL.2021.3126589.

[34] M. Turzyński, *Falowniki napięcia z quasi-rezonansowym obwodem pośredniczącym w układach napędowych, Wydanie I*. Gdańsk: Wydawnictwo Politechniki Gdańskiej, 2020.

[35] J. Everts, F. Krismer, J. Van Den Keybus, J. Driesen, and J.W. Kolar, "Optimal ZVS Modulation of Single-Phase Single-Stage Bidirectional DAB AC–DC Converters," *IEEE Trans. Power Electron.*, vol. 29, no. 8, pp. 3954–3970, Aug. 2014, doi: 10.1109/TPEL.2013.2292026.

[36] R. Li and D. Xu, "A Zero-Voltage Switching Three-Phase Inverter," *IEEE Trans. Power Electron.*, vol. 29, no. 3, pp. 1200-1210, March 2014, doi: 10.1109/TPEL.2013.2260871.

[37] R. Barlik, M. Nowak, and P. Grzejszczak, "Power transfer analysis in a single phase dual active bridge," *Bull. Pol. Acad. Sci. Tech. Sci.*, vol. 61, pp. 809–828, 2013, doi: 10.2478/bpasts-2013-0088.

[38] S. Bachman, M. Turzyński, and M. Jasiński, "Modern control strategy of bidirectional DAB converter with consideration of control nonlinearity," *Sterowanie w Energoelektronice i Napędzie Elektrycznym "SENE 2023"*, Łódź 2023.

[39] M. Gierczyński, "Analiza pracy przekształtnika DC/DC o topologii DAB z filtrem prądu oraz synteza układu regulacji w przypadku modulacji z pojedynczym przesunięciem fazowym," doctoral thesis, Warsaw University of Technology, Warsaw 2020.

[40] S. Dutta and S. Bhattacharya, "A method to measure the DC bias in high frequency isolation transformer of the dual active bridge

DC to DC converter and its removal using current injection and PWM switching," in *2014 IEEE Energy Conversion Congress and Exposition (ECCE)*, Pittsburgh, USA, Sep. 2014, pp. 1134–1139. doi: 10.1109/ECCE.2014.6953527.

[41] J. Wisniewski, S. Baba, and M. Jasinski, "Reliability demonstration of High-Performance Power Supply after IC vendor replacement," in *2021 IEEE 19th International Power Electronics and Motion Control Conference (PEMC)*, Gliwice, Poland, Apr. 2021, pp. 363–367. doi: 10.1109/PEMC48073.2021.9432635.

[42] X. Liu, M. Han, D. Liu, Z. Li, Z. Dong, and Z. Zhang, "A New Start-up Method for Dual Active Bridge Power Converters," in *2022 IEEE 5th International Electrical and Energy Conference (CIEEC)*, Nangjing, China, May 2022, pp. 4266–4270. doi: 10.1109/CIEEC54735.2022.9846100.

[43] Y.-S. Noh, D. Joo, B.J. Hyon, J.S. Park, J.-H. Kim, and J.-H. Choi, "Development of 3-phase Current-fed Dual Active Bridge Converter for Bi-Directional Battery Charger Application," in *2020 IEEE Energy Conversion Congress and Exposition (ECCE)*, Detroit, USA, Oct. 2020, pp. 2287–2290. doi: 10.1109/ECCE44975.2020.9236393.

[44] R. Kondo, P. Schulting, A.H. Wienhausen, and R.W. De Doncker, "An Automated Component-Based Hardware Design of a Three-Phase Dual-Active Bridge Converter for a Bidirectional On-Board Charger," in *2020 IEEE Energy Conversion Congress and Exposition (ECCE)*, Detroit, USA, Oct. 2020, pp. 850–857. doi: 10.1109/ECCE44975.2020.9236190.

[45] D. Bundgen, A. Thonnessen, N. Fritz, T. Kamp, and R.W. De Doncker, "Highly Integrated 200 kW SiC Three-Phase Dual-Active-Bridge Converter with 3D-Printed Fluid Coolers," in *2021 IEEE 8th Workshop on Wide Bandgap Power Devices and Applications (WiPDA)*, Redondo Beach, USA, Nov. 2021, pp. 182–187. doi: 10.1109/WiPDA49284.2021.9645076.

[46] B. Khanzadeh, T. Thiringer, and Y. Serdyuk, "Analysis and Improvement of Harmonic Content in Multi-level Three-phase DAB Converters with Different Transformer Windings Connections," in *2022 International Power Electronics Conference (IPEC-Himeji 2022- ECCE Asia)*, Himeji, Japan, May 2022, pp. 2653–2658. doi: 10.23919/IPEC-Himeji2022-ECCE53331.2022.9807076.

[47] A. Aouiti, A. Soyed, and F. Bacha, "Control and Study of the Bidirectional Three Phase DAB Converter," in *2022 8th International Conference on Control, Decision and Information Technologies* (CoDIT), Istanbul, Turkey, May 2022, pp. 1008–1013. doi: 10.1109/CoDIT55151.2022.9804020.

[48] A. Tong, L. Hang, G. Li, and J. Huang, "Nonlinear characteristics of DAB converter and linearized control method," in *2018 IEEE Applied Power Electronics Conference and Exposition* (APEC), San Antonio, TX, USA, Mar. 2018, pp. 331–337. doi: 10.1109/APEC.2018.8341031.

[49] F. Rodriguez, D.O. Garrido, R.O. Nunez, G.G. Oggier, and G.O. Garcia, "Feedback Linearization Control of a Dual Active Bridge Converter Feeding a Constant Power Load," in *2022 IEEE Biennial Congress of Argentina (ARGENCON)*, San Juan, Argentina, Sep. 2022, pp. 1–8. doi: 10.1109/ARGENCON55245.2022.9940123.

[50] M. Gierczynski, L.M. Grzesiak, and A. Kaszewski, "Cascaded Voltage and Current Control for a Dual Active Bridge Converter with Current Filters," *Energies*, vol. 14, no. 19, p. 6214, Sep. 2021, doi: 10.3390/en14196214.

[51] K.J. Hartnett, J.G. Hayes, M.G. Egan, and M.S. Rylko, "CCTT-Core Split-Winding Integrated Magnetic for High-Power DC–DC Converters," *IEEE Trans. Power Electron.*, vol. 28, no. 11, pp. 4970–4984, Nov. 2013, doi: 10.1109/TPEL.2013.2240394.

[52] L. Li, G. Xu, D. Sha, Y. Liu, Y. Sun, and M. Su, "Review of Dual-Active-Bridge Converters with Topological Modifications," in *IEEE Trans. Power Electron.*, vol. 38, no. 7, pp. 9046–9076, July 2023, doi: 10.1109/TPEL.2023.3258418.